

Holographic mode-selective launch for bandwidth enhancement in multimode fiber

Angela Amphawan^{1,2,*}

¹InterNetWorks Research Group, School of Computing, Universiti Utara Malaysia, 06010 Sintok, Kedah, Malaysia

²Department of Engineering Science, University of Oxford, Parks Road, Oxford, OX1 3PJ, UK

*a.amphawan@seh.oxon.org

Abstract: With rapidly growing bandwidth demands in Local Area Networks, it is imperative to support next generation speeds beyond 40Gbit/s. Various holographic optimization techniques using spatial light modulators have recently been explored for adaptive channel impulse response improvement of MMF links. Most of these experiments are algorithmic-oriented. In this paper, a set of lenses and a spatial light modulator, acting as a binary amplitude filter, played the pivotal role in generating the input modal electric field into a graded-index MMF, rather than algorithms. By using a priori theoretical information to generate the incident modal electric field at the MMF, the bandwidth was increased by up to 3.4 times.

© 2011 Optical Society of America

OCIS codes: (060.0060) Fiber optics and optical communications; (090.0090) Holography; (050.0050) Diffraction and gratings.

References and links

1. S. Bois, *Next Generation Fibers and Standards* (Corning Optical Fiber 2009).
2. R. J. Shapiro, "The Internet's Capacity To Handle Fast-Rising Demand for Bandwidth," USIA White Paper, (2007).
3. S. Xirasagar, *Traffic Management for Emerging (Networks Next Generation Networks , 2010)*.
4. Cisco, "Hyperconnectivity and the Approaching Zettabyte Era," Cisco White Paper (2010).
5. K. McCabe, *IEEE Launches Next Generation of High-Rate Ethernet with New IEEE 802.3ba Standard* (IEEE, 2010).
6. I. Gasulla, and J. Capmany, "1 Tb/s x km multimode fiber link combining WDM transmission and low-linewidth lasers," *Opt. Express* **16**(11), 8033–8038 (2008).
7. X. J. Gu, W. Mohammed, and P. W. Smith, "Demonstration of all-fiber WDM for multimode fiber local area networks," *IEEE Photon. Technol. Lett.* **18**(1), 244–246 (2006).
8. T. Shimada, N. Sakurai, and K. Kumozaki, "WDM access system based on shared demultiplexer and MMF links," *J. Lightwave Technol.* **23**(9), 2621–2628 (2005).
9. Z. Haas, and M. A. Santoro, "A mode-filtering scheme for improvement of the bandwidth-distance product in multimode fiber systems," *J. Lightwave Technol.* **11**(7), 1125–1131 (1993).
10. S. Berdagué, and P. Facq, "Mode division multiplexing in optical fibers," *Appl. Opt.* **21**(11), 1950–1955 (1982).
11. F. Dubois, P. Emplit, and O. Hugon, "Selective mode excitation in graded-index multimode fiber by a computer-generated optical mask," *Opt. Lett.* **19**(7), 433–435 (1994).
12. D. Erni, M. Jungo, and W. Baechtol, "Segmented VCSEL contact geometry for active coupling efficiency enhancement," in *Workshop on Compound Semiconductor Devices and Integrated Circuits (WOCSDICE)*, (Photonics Communication Group, Swiss Federal Institute of Technology (ETHZ), 2003), 67–68.
13. P. Facq, F. De-Fornel, and F. Jean, "Tunable single-mode excitation in multimode fibres," *Electron. Lett.* **20**(15), 613–614 (1984).
14. L. Raddatz, I. H. White, D. G. Cunningham, and M. C. Nowell, "An experimental and theoretical study of the offset launch technique for the enhancement of the bandwidth of multimode fiber links," *J. Lightwave Technol.* **16**(3), 324–331 (1998).
15. A. Amphawan, F. Payne, D. O'Brien, and N. Shah, "Derivation of an analytical expression for the power coupling coefficient for offset launch into multimode fiber," *J. Lightwave Technol.* **28**(6), 861–869 (2010).
16. K. Balemorthy, A. Polley, and S. E. Ralph, "Electronic equalization of multikilometer 10-Gb/s multimode fiber links: mode-coupling effects," *J. Lightwave Technol.* **24**(12), 4885–4894 (2006).
17. C. Xia, M. Ajaonkar, and W. Rosenkranz, "On the performance of the electrical equalization technique in MMF links for 10-gigabit ethernet," *J. Lightwave Technol.* **23**(6), 2001–2011 (2005).
18. D. Lenz, B. Rankov, D. Erni, W. Bachtold, and A. Wittneben, "MIMO Channel for Modal Multiplexing in Highly Overmoded Optical Waveguides," in *International Zurich Seminar on Communications (IZS)*, (IEEE, 2004)

19. J. E. Midwinter, "The prism-taper coupler for the excitation of single modes in optical transmission fibres," *Opt. Quantum Electron.* **7**(4), 297–303 (1975).
20. S. Zemon, and D. Fellows, "Tunneling leaky modes in a parabolic index fiber," *Appl. Opt.* **15**(8), 1936–1941 (1976).
21. E. Alon, V. Stojanovic, J. M. Kahn, S. Boyd, and M. Horowitz, "Equalization of modal dispersion in multimode fiber using spatial light modulators," in *GLOBECOM '04. IEEE Global Telecommunications Conference*, (IEEE, 2004), 1023–1029.
22. P. L. Neo, J. P. Freeman, and T. D. Wilkinson, "Modal Control of a 50 μ m core diameter Multimode Fiber Using a Spatial Light Modulator," in *Optical Fiber Communication and the National Fiber Optic Engineers Conference, 2007. OFC/NFOEC 2007. Conference on*, (Optical Society of America, 2007), 1-3.
23. R. A. Panicker, J. M. Kahn, and S. P. Boyd, "Compensation of Multimode Fiber Dispersion Using Adaptive Optics via Convex Optimization," *J. Lightwave Technol.* **26**(10), 1295–1303 (2008).
24. R. A. Panicker, and J. M. Kahn, "Algorithms for Compensation of Multimode Fiber Dispersion Using Adaptive Optics," *J. Lightwave Technol.* **27**(24), 5790–5799 (2009).
25. M. B. Shemirani, and J. M. Kahn, "Compensation of Multimode Fiber Dispersion by Optimization of Launched Amplitude, Phase, and Polarization," *J. Lightwave Technol.* **28**(14), 2084–2095 (2010).
26. M. B. Shemirani, J. P. Wilde, and J. M. Kahn, "Adaptive Compensation of Multimode Fiber Dispersion by Control of Launched Amplitude, Phase, and Polarization," *J. Lightwave Technol.* **28**(18), 2627–2639 (2010).
27. G. Stepniak, L. Maksymiuk, and J. Siuzdak, "Increasing Multimode Fiber Transmission Capacity by Mode Selective Spatial Light Phase Modulation," in *36th European Conference on Optical Communications*, 2010.
28. A. Flatman, "In-Premises Optical Fibre Installed Base Analysis 2007," (LAN Technologies UK, Orlando, 2004).
29. P. Bell, "Fiber Selection Guide for Premises Networks," Bell White Paper (2007).
30. A. Palmentieri, and E. Verdonik, Thorlabs (personal communication, 2007).
31. M. A. A. Neil, T. Wilson, and R. Juskaitis, "A wavefront generator for complex pupil function synthesis and point spread function engineering," *J. Microsc.* **197**(3), 219–223 (2000).
32. A. W. Snyder, and J. D. Love, *Optical waveguide theory*, Science paperbacks; 190 (Chapman and Hall, London, 1983), pp. viii, 734.
33. O. Shapira, A. F. Abouraddy, J. D. Joannopoulos, and Y. Fink, "Complete modal decomposition for optical waveguides," *Phys. Rev. Lett.* **94**(14), 143902 (2005).
34. G. T. Mase, and G. E. Mase, *Continuum mechanics for engineers*, 2nd ed. / G. Thomas Mase, George E. Mase. ed. (CRC Press, Boca Raton, Fla.; London, 1999), p. 377 p.
35. G. B. Arfken, and H. J. Weber, *Mathematical methods for physicists*, 5th ed. ed. (Harcourt Academic, San Diego, Calif.; London, 2001), pp. xiv, 1112 p.
36. R. Aris, *Vectors, tensors, and the basic equations of fluid mechanics* (Dover, 1989), pp. xiv, 286.
37. G. Keiser, *Optical Fiber Communications* (McGraw-Hill, New York, 1983).
38. R. Olshansky, "Effect of the cladding on pulse broadening in graded-index optical waveguides," *Appl. Opt.* **16**(8), 2171–2174 (1977).
39. A. Gholami, Z. Toffano, A. Destrez, S. Pellevrault, M. Pez, and F. Quentel, "Optimization of VCSEL Spatiotemporal Operation in MMF Links for 10-Gb Ethernet," *IEEE J. Sel. Top. Quantum Electron.* **12**(4), 767–775 (2006).

1. Introduction

Multimode fiber (MMF) is the established medium of choice in local area network (LAN) backbones [1]. With the advent of multimedia-rich applications such as video streaming, teleconferencing, live television, photo sharing and online video games, current MMF technology may soon overwhelm the MMF infrastructure [2–4]. With rapidly growing network demands, it is imperative to support next generation speeds beyond 40Gbit/s [5]. Many techniques have been investigated. These include wavelength division multiplexing [6–8], mode-selective launches [9–13], holographic optimization [9–13], offset launching [14,15], and electronic dispersion compensation (EDC) [16,17].

In mode-selective launches, only a subset of propagating modes is excited, in order to mitigate modal dispersion. Previous experiments on selective mode excitation include laser driving schemes [12,18], masks for spatially filtering [10,11] and prism coupling [19,20].

Recent holographic optimization experiments demonstrate the agility of spatial light modulators (SLMs) in mitigating the mode switching limitations of the static computer-generated masks [11] and the pierced plates [10]. The incident electric field at the MMF input endface may be swiftly customized by changing the hologram using a computer. Furthermore, the rapid reconciliation speed of the SLM allows for adaptive updating of the incident field on the MMF [21]. It has been recently demonstrated that the channel impulse response or bandwidth of the MMF link was improved by means of holographic optimization using an SLM [21,22].

Most holographic mode-selective launches are algorithmically intensive [21–26]. In this work, as in [27], lenses played the pivotal role in generating the input modal electric field into a graded-index MMF, rather than algorithms. In [27], the SLM functions as a binary phase filter, whereas here, the SLM functions as a binary amplitude filter. In both, the transmittance of the filter is a function of the inverse Fourier transform of the transverse modal field distribution. Also, in both, a priori theoretical information on the modal electric field in MMF was used instead of a random estimate at the onset of the bandwidth optimization process. It is shown that using the proposed technique for mode-selective launch, the bandwidth was increased by more than 3 times. This agrees with the results achieved in [27] using a binary phase filter.

Apart from offering a new experimental approach for mode-selective launching, this work also examines the modal decomposition of the received signal at the output of a graded-index MMF. While the modal analysis of the retrieved output modes plays an important role in understanding the effects of power modal coupling within the channel, no special focus has been given to this in previous mode-selective launches. To pave the way towards better quantitative understanding of power coupling effects within the channel, the method and results for a noninterferometric modal decomposition technique are presented. The results of the modal decomposition are also used to analyze the channel impulse response and estimate the improvement in the bandwidth compared to the bandwidth from a conventional launch.

The experimental setup and method will be discussed in Section 2. The modal decomposition and bandwidth analysis will then be presented in Sections 3 and 4 respectively.

2. Holographic mode-selective launch experiment

2.1. Experimental setup

The experimental setup is shown in Fig. 1. A 128x128 pixel transmissive binary amplitude spatial light modulator (SLM) and a combination of three lenses were used. The lenses consist of achromatic doublets of focal lengths $f_1 = 300\text{mm}$ ($L1$) and $f_2 = 100\text{mm}$ ($L2$); and a fiber collimator with an aspheric lens of $f_3 = 11\text{mm}$ ($L3$). A 632.8nm Helium Neon laser was used. A visible laser was chosen for ease of alignment of optics and to easily measure the generated modal field at various points along the system. Considering that a majority of MMF in LANs is less than 1km [28,29], a MMF length of 1km was chosen for the experiment. The MMF used was a 1km-long graded-index Thorlabs GIF625, with a refractive index profile parameter, $\alpha = 1.81$ [30] and a core diameter of $62.5\mu\text{m}$.

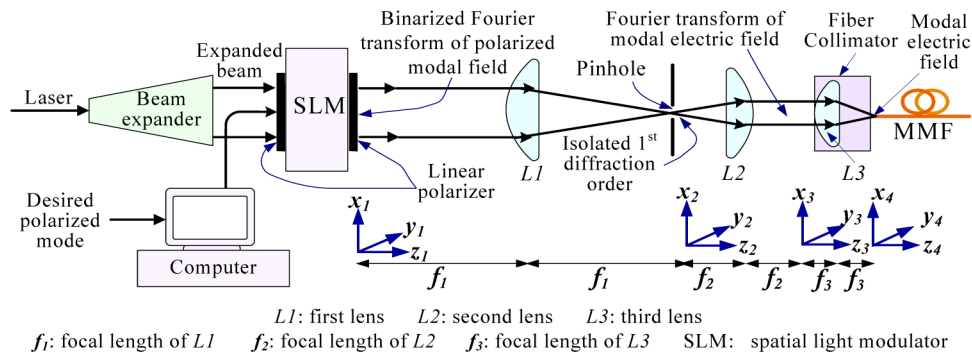


Fig. 1. Experimental setup for holographic selective mode excitation.

2.2. Mathematical description

The experimental technique for the holographic mode-selective launch is adapted from a microscopy technique by Neil et al. [31] for generating a complex electric field for tuning the pupil function of the objective lens in a confocal microscope. The experimental technique in

[31] was modified in order to create the electric field of linearly polarized modes of a perfect infinite parabolic MMF for the selective launch. In our experiment, instead of two lenses as in [11] and [31], three lenses were used for gradual field reduction in order to reduce spherical aberration of the generated modal electric field. This increases power coupling efficiency at the input. Hence, for the hologram, instead of encoding the desired electric field itself as in [31], here, the Fourier transform of the desired electric field will be encoded in the hologram. A summary of the technique used for generating the modal electric field of is given in Fig. 2.

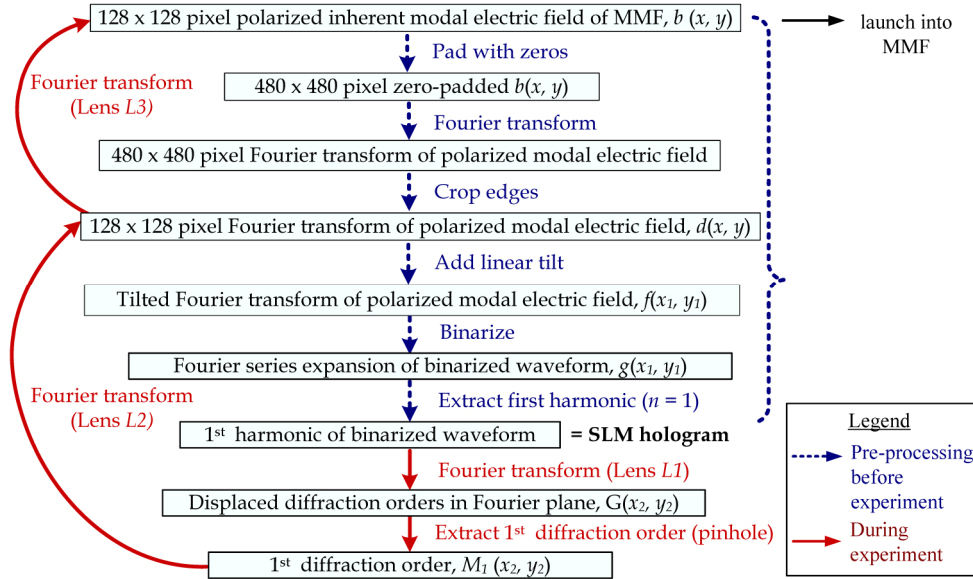


Fig. 2. Summary of technique used for generation of modal electric field of an infinite parabolic MMF.

The transverse electric field for the LPLm mode of a weakly-guiding infinite parabolic MMF, elm is composed of two orthogonal polarizations:

$$b = F \sin l\phi, \quad (1)$$

$$b = F \cos l\phi. \quad (2)$$

F is the radial dependence of the transverse electric field, given by [32]:

$$F = R^l L_{m-1}^{(l)}(VR^2) \exp(-0.5VR^2), \quad (3)$$

where R is the normalized core radius, ϕ is azimuthal angle in the plane of the MMF core, V is the normalized frequency, $L_{m-1}^{(l)}$ is the generalized Laguerre polynomial, l is the azimuthal mode number and m is the radial mode number.

First, for the mode to be launched, the Fourier transform of any polarization of the transverse modal electric field in Eqs. (1) and (2) is taken. Then, a linear tilt is added to the Fourier transformed field. This yields the complex field:

$$f(x_1, y_1) = d(x_1, y_1) \exp[j(\tau_x x_1 + \tau_y y_1)], \quad (4)$$

where x_1 and y_1 are spatial coordinates shown in Fig. 1, $d(x_1, y_1)$ is the polarized Fourier transform of the polarized modal electric field; τ_x and τ_y are linear tilt constants in the Fourier plane in the horizontal and vertical directions respectively. The tilting facilitates the

The tilting facilitates the isolation of the first diffraction order by spatially separating the higher diffraction orders from the center of the Fourier plane.

Following this, the phase of the complex field $f(x_1, y_1) = u(x_1, y_1) + jv(x_1, y_1)$ is binarized according to the amplitude mapping shown in Fig. 3, adapted from [31]. The binarized modal field is then displayed on the SLM. The binarized waveform may be expressed as a series of harmonics in a Fourier series expansion:

$$g(x_1, y_1) = a_0 + \frac{4}{\pi} \sum_{n=1}^{\infty} a_n \cos\{n[\xi(x_1, y_1) + \tau_x x_1 + \tau_y y_1]\}, \quad (5)$$

where $a_0 = 2\alpha(x_1, y_1)\pi - 1$ is the constant term and $a_n = \sin[n\alpha(x_1, y_1)]/n$ is the Fourier cosine coefficient of the Fourier series expansion. L1 then takes the Fourier transform of the binarized modal field on the SLM. Taking the Fourier transform of Eq. (5) yields:

$$G(x_2, y_2) = M_o(x_2, y_2) + \sum_{n=1}^{\infty} [M_n(x_2 + n\tau_x, y_2 + n\tau_y) + M_n^*(n\tau_x - x_2, n\tau_y - y_2)], \quad (6)$$

where x_2 and y_2 are spatial coordinates in the Fourier plane of L1 as shown in Fig. 1, * is the complex conjugate and $M_n(x_1, y_1)$ is the n -th diffraction order. The effect of the tilt is to separate the diffraction orders by multiples of the tilt constants in the Fourier plane. The first diffraction order, M_1 is then spatially filtered using a pinhole located in the back focal plane of L1. M_1 is a magnified version of the original polarized modal electric field $b(x, y)$.

The telecentric L2-L3 combination scales the magnified modal electric field by a reduction factor given by the conjugate ratio of L2 and L3. The input endface of the MMF is placed in the back focal plane of L3 to couple the generated modal electric field. The applied tilt is removed by moving the two lenses laterally in order to accommodate for the deviation in the direction of propagation of M_1 from the original Fourier plane axis. The generated theoretical modal electric field is then optimized for improving the power coupling efficiency.

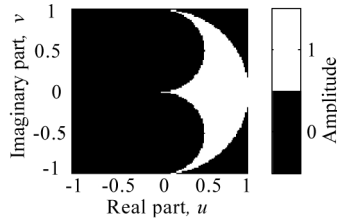


Fig. 3. The mapping of a complex field onto the required amplitude, adapted from [31].

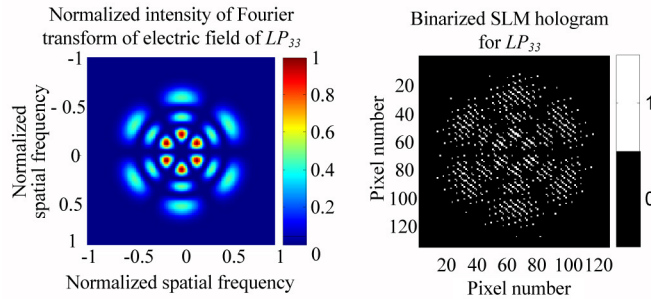


Fig. 4. Fourier transform of electric field of LP33 and corresponding binarized SLM hologram.

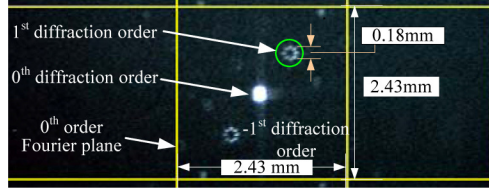


Fig. 5. Measured intensity distribution of Fourier plane of L1 for LP41 mode and location of first diffraction order.

2.3. Experimental demonstration of holographic mode-selective excitation

Prior to the experiment, the binarized SLM hologram for the desired mode was generated using MATLAB. The steps are summarized in Fig. 2. First, a 128x 128-pixel array of the linearly polarized modal electric field of the desired mode was simulated. The array was then zero-padded to 480 x 480 pixels before taking the Fourier transform. The zero-padding increases the discernibility of fine details in the Fourier plane. The empty edges of the 480 x 480 pixel Fourier plane were then cropped to obtain an array of 128 x 128 pixels to match the number of pixels on the SLM. The array was then tilted and binarized according to Fig. 3, as described in Section 2.2. Fig. 4 illustrates a typical Fourier transformed modal electric field pattern and the corresponding binarized pattern for the SLM. The binary hologram of the desired mode was displayed on the SLM. A collimated beam from the laser was expanded and directed through the SLM. The binarized hologram was Fourier transformed by L1. An example of the Fourier plane of L1 and the location of the first diffraction order is shown in Fig. 5, for the excitation of LP41. A 0.2mm diameter pinhole was then used to isolate the first diffraction order. The first diffraction order was then scaled to the inherent size of the modal electric field of the MMF by L2 and L3. The amplitude and phase of the generated modal electric field were measured before the launch. The power coupling efficiency into the desired mode at the input of the MMF is given by:

$$c_{lm\ in} = \left| \iint_{A_{core}} \mathbf{E}_{in}(x, y) \mathbf{e}_{lm}^*(x, y) dx dy \right|^2 \left/ \iint_{A_{core}} |\mathbf{E}_{in}(x, y)|^2 dx dy \iint_{A_{core}} |\mathbf{e}_{lm}(x, y)|^2 dx dy \right., \quad (7)$$

where \mathbf{E}_{in} is the generated electric field of the desired mode at the input and \mathbf{e}_{lm} is the polarized transverse electric field for LP $_{lm}$ of a weakly-guiding infinite parabolic MMF. LP $_{lm}$ modes within the range of $l = 0, 1, \dots, 4$ and $m = 1, 2, \dots, 4$ were excited. The power coupling efficiencies of the generated modal electric fields were in the range of 90.15% to 95.79%. Thus, the generated modal electric field is a close approximate of the theoretical modal electrical field. The power loss may be due to the slight misplacement of the pinhole for isolation of the first diffraction order or the misalignment of the lenses to accommodate for the change in the direction of the propagation of the first diffraction order with respect to the zeroth diffraction order. The power coupling efficiency at the input is the percentage of the generated modal electric which was coupled into the MMF at the input assuming no insertion loss.

The MMF was connected to a fiber collimator, located in the back focal plane of L3. This couples the generated electric field into the MMF. The generated modal electric field provides a priori information for the optimization process. It is noted that although a perfect infinite parabolic refractive index profile ($\alpha = 2$) was assumed in calculating the theoretical modal electric field and used for generating the incident modal electric field at the input enface of the MMF, it is shown in [15] that the effect of the refractive index profile parameter, α on the modal electric field distribution for manufactured MMFs with a finite cladding ($1.8 < \alpha < 2.2$) is negligible. For maximum power coupling at the output, the diameter, x , y , and z positions, tilt and yaw of the generated modal electric field at the input has to be matched to those of the inherent modal electric field of the MMF used. Thus, for each of these parameters, a small

change in the value was introduced at each iteration while the values for other parameters were maintained. This was followed by the calculation of the channel impulse response width. The particular parameter was varied until the squared error between the previous channel impulse width and the current channel impulse width was less than 1×10^{-6} . This was repeated for all the aforementioned parameters. The optimization is complete when all the aforementioned parameters have been adjusted such that the squared error between the previous channel impulse width and the current channel impulse width is less than 1×10^{-6} . A typical set of the final measured output intensity distributions is shown in Fig. 6.

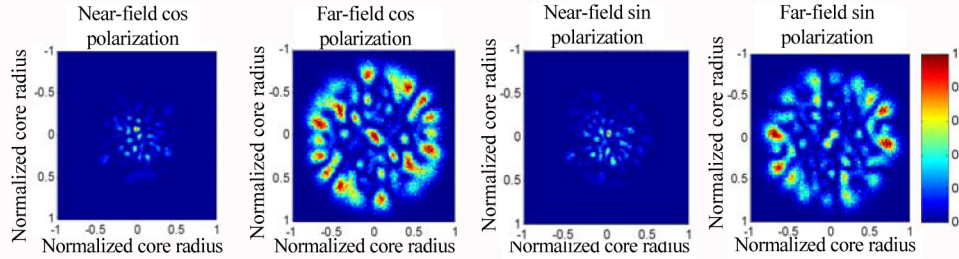


Fig. 6. A set of four measured output intensity distributions for the noninterferometric modal decomposition of selective excitation of LP44 mode at the output of the MMF.

For the range of modes excited, it was found that about 3 to 4 iterations were required when a priori information of the theoretical modal electric field in graded-index MMF was used at the onset of the optimization process. As a comparison, a random modal electric field estimate was used at the onset of the optimization process. It was found that 14 to 20 iterations were required. This agrees with the results in [22] for another holographic selective mode excitation setup where no a priori information was injected into the system during the optimization process. Thus, this demonstrates that a 15% to 28% reduction in the number of iterations was achieved when a priori information of the modal electric field of the MMF is introduced at the onset of the optimization process.

3. Modal decomposition of output field

At the MMF output, the power coupling coefficient into any given mode is determined by the normalized overlap integral of the electric field at the output and the transverse electric field for LP l_m mode [32]. For this experiment, a noninterferometric modal decomposition adapted from [33] was used to retrieve the power coupling coefficients. The advantage of this technique is the lower computational requirement for acquiring the power coupling coefficient distribution compared to using the overlap integral. Also, the power coupling coefficients can be retrieved directly without interferometry. In [33], the modal decomposition for a hollow-core photonic-band gap fiber was examined. Here, the technique will be applied to an infinite parabolic silica MMF. For faster computation, several aspects of the algorithm in have been improved. Firstly, instead of using both the transverse modal magnetic and electric fields for the LP l_m modes as in [7], here, the transverse modal magnetic field, h_{lm} has been replaced by the transverse modal electric field elm using $\mathbf{h}_{lm} = (\epsilon_o/\mu_o)^{1/2} n_{co} (\hat{\mathbf{z}} \times \mathbf{e}_{lm})$ [32], where $\hat{\mathbf{z}}$ is the unit vector parallel to the MMF waveguide axis, n_{co} is the refractive index of the MMF core, ϵ_o is the free-space permittivity and μ_o is the free-space permeability. Secondly, in our derivation, the order of the indices of tensor $\Lambda_{l_1 m_1 l_2 m_2 l_3 m_3 l_4 m_4}$ was reduced from 4 to 3, by implicitly summing repeated indices [34–36] as follows:

$$\Lambda_{l_1 m_1 l_2 m_2 l_3 m_3 l_4 m_4} c_{l_3 m_3} c_{l_4 m_4}^* = \Lambda_{l_1 m_1 l_2 m_2 l_3 m_3} \quad (8)$$

Following the approach in [33], applying Eq. (8) and replacing h_{lm} by elm , for each excited mode, four images of the output intensity distribution were recorded, one for each orthogonal polarization in both the near-field and far-fields. The new error function between

the reconstructed estimate and the actual measure intensity for a weakly-guiding infinite parabolic MMF was then derived. The derived error function for an infinite parabolic MMF may be expressed as:

$$\Delta^{p,q} = \frac{1}{N^2} \sum_{l_1 m_1 l_2 m_2 l_3 m_3 l_4 m_4} c_{l_1 m_1} c_{l_2 m_2}^* c_{l_3 m_3} c_{l_4 m_4}^* \Lambda_{l_1 m_1 l_2 m_2 l_3 m_3 l_4 m_4} - \frac{2}{N} \sum_{l_1 m_1 l_2 m_2} c_{l_1 m_1} c_{l_2 m_2}^* \Gamma_{l_1 m_1 l_2 m_2}^{p,q} + P^{p,q}, \quad (9)$$

where p defines the plane of measurement; $p = 1, 2$ for the far-field and near-field planes respectively. q defines the MMF two orthogonal polarizations of the transverse electric field.

For $q = 1$, $b = \text{Flm} \cos l\phi$ and for $q = 2$, $b = \text{Flm} \sin l\phi$. N is a power normalization constant. $c_{l_n m_n}$ is the power coupling coefficient for the LPlm mode of a weakly-guiding infinite parabolic MMF at the MMF output, where the subscripts ln and mn are the n -th indices for the azimuthal and radial mode numbers respectively. The measured output power, $P^{p,q} = \int_A [I_{me}^{p,q}(x, y)]^2 dA$, whereby A is the cross-sectional area of the MMF core and I_{me} is the measured intensity distribution at the output. The measured output power takes into account the free-space path loss from the output endface of the MMF to the charged-coupled device sensor used for the power measurement. The derived tensors for a weakly-guiding infinite parabolic MMF are given by:

$$\Gamma_{l_1 m_1 l_2 m_2}^{p,q} = \int_{\text{core}} I_{me}^{p,q} \left[e_{x_{l_1 m_1}}(x, y) e_{x_{l_2 m_2}}(x, y) + e_{y_{l_1 m_1}}(x, y) e_{y_{l_2 m_2}}(x, y) \right] dA, \quad (10)$$

$$\Lambda_{l_1 m_1 l_2 m_2 l_3 m_3 l_4 m_4} = \int_{\text{A core}} \left[e_{x_{l_1 m_1}}(x, y) e_{x_{l_2 m_2}}(x, y) + e_{y_{l_1 m_1}}(x, y) e_{y_{l_2 m_2}}(x, y) \right] \times \left[e_{x_{l_3 m_3}}(x, y) e_{x_{l_4 m_4}}(x, y) + e_{y_{l_3 m_3}}(x, y) e_{y_{l_4 m_4}}(x, y) \right] dA, \quad (11)$$

where $e_{x_{l_n m_n}} = \text{Flm} \cos l\phi$, $e_{y_{l_n m_n}} = \text{Flm} \sin l\phi$. The overall error function is $\Delta = \sum_{p,q} \Delta^{p,q}$.

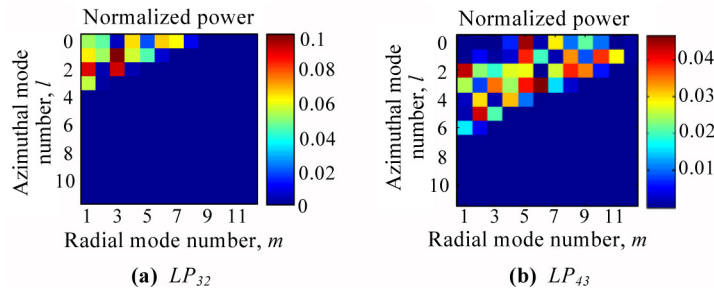


Fig. 7. Modal decomposition of output field for selective excitation of various modes.

MATLAB was used to construct the tensor function for each polarization of the output modal field in each plane using the corresponding measured intensity distribution. The MATLAB optimization toolbox was then used to minimize the total error function. Typical modal decomposition results are presented in Fig. 7. The power coupling efficiency into the desired mode generally decreases the further the mode number is from the mode number of the desired mode. Also, the effect of power modal coupling is more dominant on the radial

mode number than on the azimuthal mode number within a particular selectively excited channel. In addition to this, selective excitation of lower-ordered modes at the input exhibited less power modal coupling at the output than selective excitation of higher-ordered modes at the input.

4. Channel bandwidth estimation

To determine the bandwidth of the experimental holographic selective mode excitation channel, the channel impulse response was first calculated. In the worst-case scenario, it is assumed that complete redistribution of power occurs immediately after the generated modal field is coupled into the MMF. Under this assumption, the lowest bandwidth gain is achieved. Thus, the worst-case channel impulse response may be expressed as:

$$h(t) = \sum_{q=1}^{\infty} \eta_q \delta(t - t_q), \quad (12)$$

where $\delta(t)$ is the delta function, $q=2m+1-1$ is the mode group number, η_q is the power coupling coefficient for the q -th mode group from the modal decomposition in Section 3. t_q is the modal time delay for the q -th mode group from the formula in [37], given by the inverse of the modal group velocity for mode group q , $v_q = d\tilde{\beta}_q/d\omega$, using the profile parameter $\alpha=1.81$ and the scalar propagation constant $\tilde{\beta}_q = [v/(\rho\sqrt{2\Delta})] \sqrt{1 - 2\Delta(q/Q)^{2\alpha/(\alpha+2)}}$, where ω is the laser angular frequency, V is the normalized frequency, ρ is the core radius, Δ is the profile height parameter, R is the normalized distance from the core centre, q is the mode group number and Q is the number of mode groups in the MMF. It is shown in [38] that a finite cladding affects the modal time delays of only modes near cutoff which are expected to be attenuated rapidly along the fiber so that there is little difference between the time delay of an infinite and finite cladding fiber. Typical channel impulse responses from the experiment are shown in Fig. 8 (a)-(b).

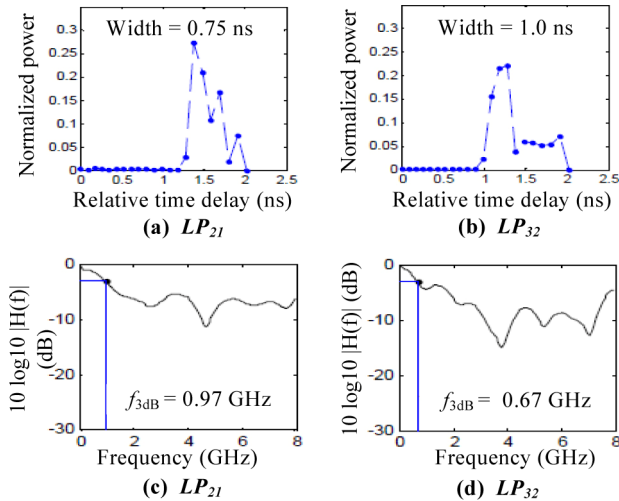


Fig. 8. Channel transfer functions for selective excitation of modes (a) LP21 and (b) LP32 and corresponding channel transfer functions (c)-(d) at 633nm wavelength.

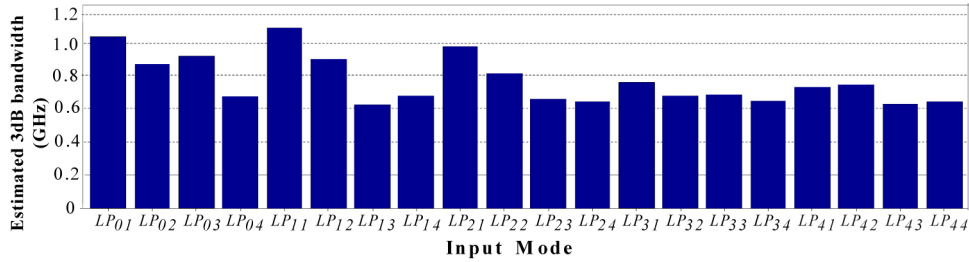


Fig. 9. Estimated 3dB channel bandwidths of holographic selective excitation of various modes.

The transfer function for each selective mode excitation channel was obtained by taking the Fourier transform of the corresponding channel impulse response. Examples of typical transfer functions are shown in Fig. 8 (c)-(d). The 3dB bandwidth for each selectively excited channel was then interpolated from the corresponding channel transfer function. A summary of the interpolated 3dB bandwidths is given in Fig. 9. The estimated 3dB bandwidths were in the range 0.62 GHz to 1.03 GHz for the range of modes excited. Specialized tests by the manufacturer for the particular MMF show that the estimated bandwidth for the 1km of GIF625 MMF used was 0.3GHz.km at 633nm [30]. Thus, it has been demonstrated that the conventional bandwidth of a MMF has been increased 2.0 to 3.4 times using the new holographic selective mode excitation technique. This agrees with the results achieved in [27] using the SLM as a binary phase filter.

There are some minor fluctuations when the measurement is repeated on consecutive days due to changes in the output modal content. The resulting bandwidth fluctuation is within 1%.

5. Conclusions

A new mode-selective launch has been demonstrated experimentally using a binary amplitude SLM and three lenses. The new approach provides an alternative means of generating the optimum input modal electric field into the MMF in order to maximize the bandwidth. The theoretical modal field of the desired mode is generated and coupled into the MMF, while maintaining a substantial amount in the same mode at the output by basic mean-square error minimization. The bandwidth was increased by up to 3.4 times while the number of iterations was reduced.

Unlike the continuous laser used in this work, the output modal distribution of a pulsed VCSEL changes during the period of the pulse and this will change the distribution of modes launched into the fiber [39]. However, as shown in [39], the VCSEL modal output is almost constant for 90% of the pulse duration, and only changes during turn-on and turn-off. This indicates that the methods described in this paper will also be applicable to pulsed VCSELs.